



Cite this: *RSC Adv.*, 2022, **12**, 30416

Received 7th July 2022
 Accepted 16th October 2022
 DOI: 10.1039/d2ra04197a
rsc.li/rsc-advances

Water characterization and structural attribution of different colored opals

Niu Li,^{ab} Qingfeng Guo,^{ID *ab} Qianqian Wang^{ab} and Libing Liao ^{ID *c}

The structure type and water content of opal will affect its stability and value. When the structure is Opal-A type, its value is higher. When the water content is high, its stability will decrease. The structural attribution and water distribution of pink, yellow, green, blue and purple opal have been investigated by several methodologies like powder X-ray diffraction (XRD), scanning electron microscopy (SEM), thermogravimetric analysis (TGA), and Fourier transform near infrared spectroscopy (FT-NIR). The results show that all the opal samples are CT type, among which the green sample has the highest crystallinity. The water contents of the opals range from 3.06 to 8.78%. The distribution and quantity of molecular water (H_2O_{mol}) and silanols (H_2O_{SiOH}) are calculated semi-quantitatively according to intensity of 4500 cm^{-1} and 5200 cm^{-1} peaks in the near infrared region, and it is found that the water in all the samples is basically composed of molecular water. The precipitation mechanism for opal formation results in different structural types, and the difference in structural composition leads to different water contents. This work provides a theoretical basis for the future study of the opal metallogenetic environment.

1. Introduction

Opal is a natural hydrated silica with the chemical formula of $SiO_2 \cdot nH_2O$. It is precipitated from saturated silicon-rich fluids by biological or abiotic processes,^{1–3} and the different formation conditions lead to different opal types with different structures. Levin and Ott⁴ used X-ray diffraction for the first time to discover the diffraction peak of cristobalite except glass. Successively, some scholars later verified that opal contains crystalline high-temperature cristobalite and low-temperature cristobalite.^{5–7} Flörke⁸ proposed the hypothesis that opal is the product of disordered paragenesis of cristobalite and tridymite. Garavelli⁹ further confirmed that opals can be divided into ordered and disordered types according to the degree of regularity of their structural arrangement. Jones and Segnit¹⁰ point out that opals can be divided into the following types, Opal-A: a state of high disorder and amorphous. Opal-CT: disordered cristobalite with varying degrees of accumulation and containing a large amount of tridymite. Opal-C: cristobalite with incomplete regular accumulation, mixed with a small amount of tridymite.

The precipitation mechanism of opal also leads to its high-water content, usually 4–10%. Hannay¹¹ explored the loss rate of internal water content of opal with the increase of temperature. Later, some scholars proposed that the water in the opal exists in the gap of the silicon spheres. However, the common opal did not have such gap of the precious opal, it is not composed of silica spheres. Many studies have shown that water in opal exists in the form of molecular water (H_2O_{mol}) and silanol groups (H_2O_{SiOH}).^{12–18} Molecular water (H_2O_{mol}) exists in the form of adsorbed water, free water molecules remaining on the surface or in the cavity (Fig. 1). Silanols (H_2O_{SiOH}) exists in the form of free silanol groups, surface or cavity free hydrogen bonding with water molecules or hydroxyl groups, and hydrogen bonding with silanol groups with the same silicon atoms (Fig. 1). Similarly, the occurrence state of water in opal is very important for a deep understanding of opal, because once the opal is mined and processed into gemstones, the subsequent loss of water whitening and cracks have a great impact on its quality.

Scholars have reported a large number of reports on the structural classification of opal and the existence form of water,^{10,19–21} but there is a lack of comparative study on the water characterization and structure attribution in different colored opals. In addition, it is difficult to identify opal color variety, what type of structure and water content by naked eyes. Accordingly, the structural attribution and water distribution of pink, yellow, green, blue and purple opal, have been investigated through several methodologies like powder X-ray diffraction (XRD), scanning electron microscope (SEM), thermogravimetric analysis (TG), Fourier transform near infrared

^aSchool of Gemmology, China University of Geosciences, Beijing, 100083, China.
 E-mail: qfguo@cugb.edu.cn

^bJewelry and Mineral Materials Laboratory of Experimental Teaching Demonstration Center, Beijing, China

^cBeijing Key Laboratory of Materials Utilization of Nonmetallic Minerals and Solid Wastes, National Laboratory of Mineral Materials, School of Materials Sciences and Technology, China University of Geosciences, Beijing 100083, China. E-mail: clayl@cugb.edu.cn



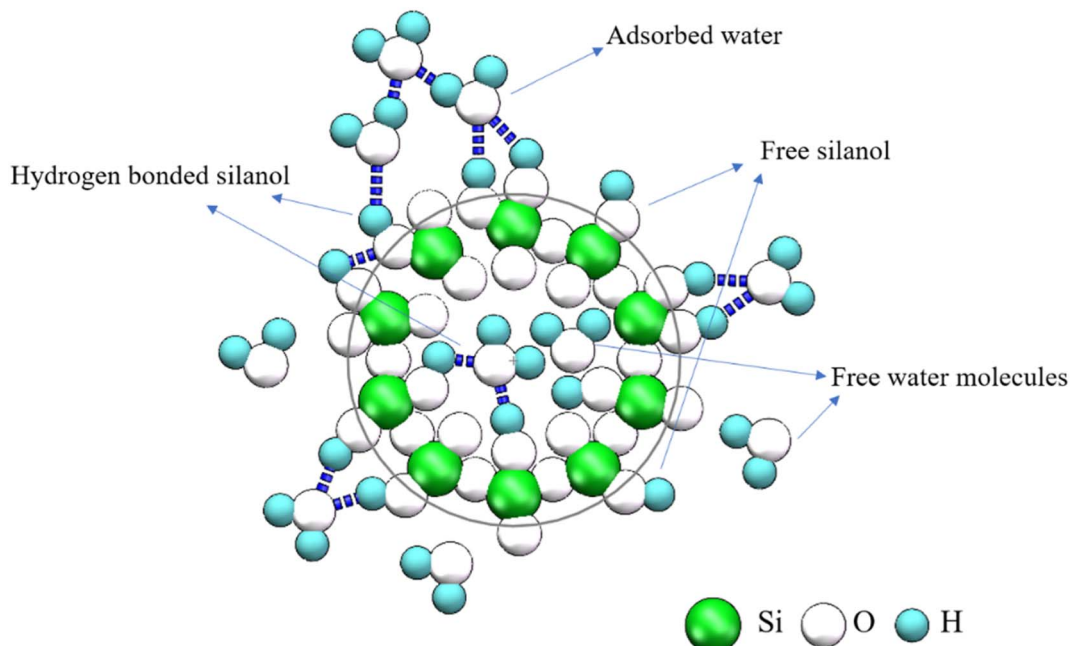


Fig. 1 Schematic diagrams of different forms of water in opal.

spectroscopy (FT-NIR) in this work. The mineralogical state of opals of different colors was obtained by structural comparison. In order to understand the stability of samples, Lambert-Beer law was used to semi-quantitatively calculate the amount of molecular water (H_2O_{mol}) and silanols (H_2O_{SiOH}) in different color samples. This study brings new data to the understanding of the hydration state of colored opal.

2. Materials and methods

2.1. Materials

Opal samples of five colors, pink, yellow, green, blue and purple, were collected in the study, ranging in size from 1 to 10 cm (Fig. 2).



Fig. 2 Front and reverse sides of five different colored opals.



2.2. Methods

Standard gemological properties of five different colored opals were determined, including refractive index, hydrostatic SG specific gravity/density, UV fluorescence (366–245 nm) and microscopic features.

The instrument used for powder X-ray diffraction test was Bruker D8 Advance from Germany, with $\text{Cu K}\alpha$ radiation and a scan speed of 4° min^{-1} , and scanning range is 5 – 80° (2θ).

Five different colored opals were examined with SUPRATM 55 type scanning electron microscope (SEM), using an electron-beam energy of 15 electron volts and a focal spot of about 0.8 nm. The samples were platinum coated before analysis.

The total water content of each opal was measured using thermo-gravimetric (TG) analysis, with a NETZSCH STA449C synchronous thermal analysis instrument. Samples (circa 5–15 mg of pieces) were loaded in Al_2O_3 crucible. Samples were heated ($10^\circ \text{ C min}^{-1}$ in a 20 ml min^{-1} flowing nitrogen atmosphere) and run between 25 and 1000 °C.

The near infrared measurements were obtained using Tensor 27 spectrometer. The sample was cut and polished into very thin slices, and tested by transmission method. The near infrared spectra of the samples were measured in the region

8000–4000 cm^{-1} at a resolution of 4 cm^{-1} . The scanning speed is 10 kHz, and total of 32 scans were carried each time.

3. Results and discussion

3.1. Gemological properties

The gemological properties and surface characters of the investigated opals are reported in Table 1. All the samples were uniformly colored with varying degrees of surrounding rock, showing a greasy-waxy luster without play of color effect were observed (Fig. 2). The refractive index for the samples is in the range of 1.44–1.45 and the values of specific gravity are ranging from 2.06 to 2.08, and these values are comparable with other opals in literatures.^{22–29} The purple sample shows green fluorescence under UV lamp. The specific gravity of pink sample is related to the inclusion of palygorskite.²² Except for the purple sample which shows green fluorescence, the other samples show inert under the UV lamp.

The microscopic observations revealed that the pink opal has a granular structure (Fig. 3a). As shown in Fig. 3b and c, the yellow opal contains white cloudy inclusions and black dendritic inclusions, and the green opal fills dendritic

Table 1 Gemological properties of the investigated opals

Sample	Color	Specific gravity	Luster	Refractive indices	Fluorescence (s)	Fluorescence (l)
Opal-P	Pink	2.12	Greasy-waxy	1.44	Weak pink	Inert
Opal-Y	Yellow	2.09	Greasy-waxy	1.44	Inert	Inert
Opal-G	Green	2.08	Greasy-waxy	1.45	Inert	Inert
Opal-B	Blue	2.06	Vitreous-greasy	1.44	Inert	Inert
Opal-Pur	Purple	2.08	Greasy-waxy	1.45	Vivid green	Weak green

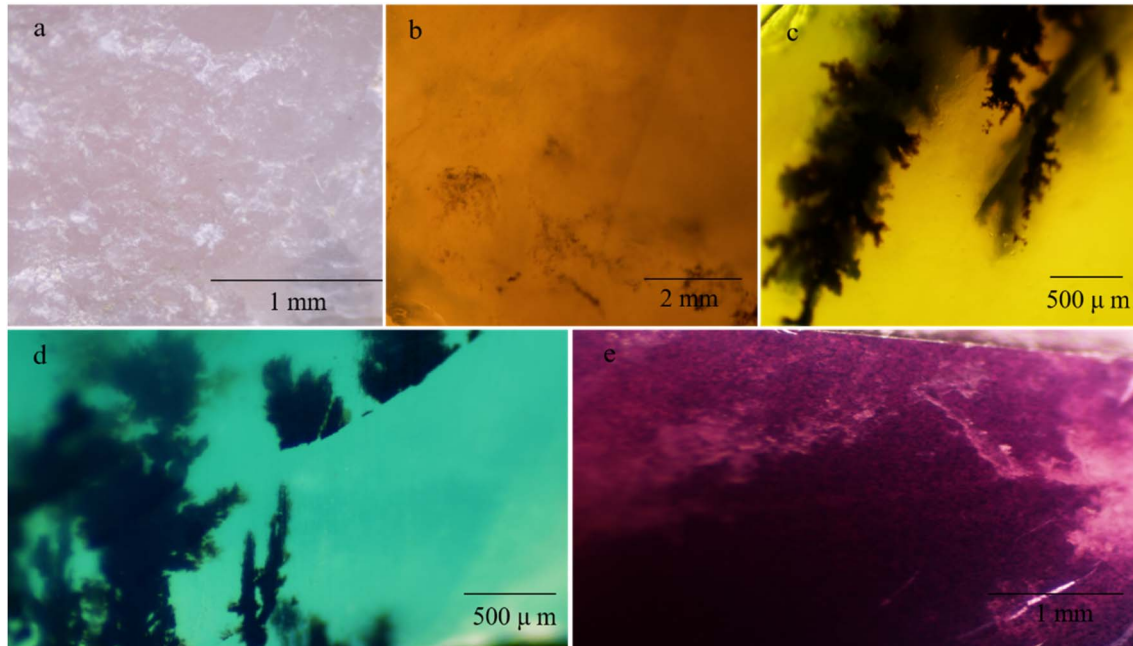


Fig. 3 Pictures of samples of opals observed under the microscope. (a) Pink opal; (b) yellow opal; (c) green opal; (d) blue opal; (e) purple opal.



inclusions. The texture of blue opal is fine and contains dendritic inclusions (Fig. 3d), and purple opal revealed the inhomogeneous nature of the material, with purple spots (Fig. 3e).

3.2. X-ray powder diffraction analysis

Fig. 4 shows the XRD patterns of opals with different colors. $\sim 4.3 \text{ \AA}$ (around $20.65^\circ 2\theta$) acromion is often accompanied by $\sim 4.1 \text{ \AA}$ (around $21.5^\circ 2\theta$) diffraction peak. The more disordered the structure is, the greater the intensity ratio of diffraction peaks at 4.3 \AA and 4.1 \AA is.³⁰ Some scholars think that the diffraction peak at 4.3 \AA is not only related to the (040) plane of tridymite and the (101) plane of cristobalite, but also the diagnostic peak of Opal-CT.^{10,31,32} The appearance of the diffraction peak at 4.3 \AA reveals the cristobalite in the opal is in a low temperature state.³³ The d value is ranging from 4.261 to 4.321 \AA in the opal samples.

The diffraction peak of $\sim 4.1 \text{ \AA}$ (around $21.6^\circ 2\theta$) is the highest peak of opal, which is considered to be caused by the juxtaposition of cristobalite (101) plane and tridymite (404) plane.³⁴ The order degree of opal structure can be diagnosed by 4.1 \AA offset position. The standard Opal-CT type opal will show a typical diffraction peak of 4.09 \AA . The d value of Opal-C type opal is between 4.01 and 4.05 \AA , while Opal-CT is characterized by a shift in the d value of the Opal-C ranging from 4.06 to 4.11 \AA .^{22,35-37} The d values at around 21.6° is ranging from 4.095 to 4.110 \AA . The ratio of cristobalite to tridymite can be calculated

by comparing the position of the characteristic peak in the range of $d = 4.04$ – 4.11 \AA (Table 2) (Opal-C contains 20–30% tridymite, Opal-CT > 50%). The following formula can be used:²¹

$$C/T_{\text{XRD}} = (d_{\text{trid}} - d_{\text{measured}})/(d_{\text{trid}} - d_{\text{crist}}) = (4.11 \text{ \AA} - x)/(4.11 \text{ \AA} - 4.04 \text{ \AA})$$

where x is the d value of different colored opals at $\sim 21.6^\circ 2\theta$.

The diffraction peak of $\sim 2.5 \text{ \AA}$ (around $35.8^\circ 2\theta$) is composed by the juxtaposition of the tridymite at 2.52 \AA (–341) and the cristobalite at 2.48 \AA (200).^{30,38,39} Previous studies have confirmed that the offset peak range of Opal-CT at $\sim 35.8^\circ$ is 2.49 – 2.52 \AA , and that of Opal-C is 2.48 – 2.49 \AA .^{40,41} The diffraction peak of $\sim 2.5 \text{ \AA}$ is also of great significance for the diagnosis of opal structural order degree, and some authors proposed that 2.5 \AA is more accurate than the main peak 4.1 \AA .⁴² In addition, there is a certain correlation between the full width at half maximum (FWHM) of 2.5 \AA diffraction peak and the crystal size.⁴³ The d values of $\sim 2.5 \text{ \AA}$ is ranging from 2.489 to 2.506 \AA . The average grain size of the crystal plane is calculated by Jade software according to the d value at 2.5 \AA , as shown in Table 2.

The peak value of $\sim 2.03 \text{ \AA}$ (around $44.3^\circ 2\theta$) is caused by the juxtaposition of the (–432) plane of tridymite and the (202) plane of cristobalite. Fig. 4 shows that the peak at around 44.3° is not clear, which is caused by the inclusion of palygorskite. Although this peak is very weak, it can provide evidence for the order of opal. In some experiments, the appears of 2.03 \AA together with big particles.⁴³ The d value of this diffraction peak is ranging from 2.045 to 2.049 \AA .

The diffraction peak of $\sim 1.6 \text{ \AA}$ (around $56.6^\circ 2\theta$) is also caused by the juxtaposition of the (–513) plane of tridymite and (301) plane of cristobalite. Although the intensity of this peak is very weak, it can be used as a characteristic of opal in specific minerals.⁴¹ The d value of this diffraction peak is ranging from 1.609 to 1.617 \AA .

Besides the previous peaks, diffraction peaks related to other secondary minerals were also detected. The quartz diffraction peak in auxiliary phase is slightly higher in Opal-Pur. Opal-P contains abundant diffraction peaks of palygorskite.^{22,44,45} The fluorite peak in Opal-Pur is consistent with the characteristic peak of calcium fluoride numbered R040099 in RUFF database.

XRD results show that all the d value at $\sim 21.6^\circ$ are bigger than 4.05 \AA , at the same time, combined with the ratio of cristobalite to tridymite, all opal samples can be defined to Opal-CT type. All samples have a 4.3 \AA diffraction peak, which means that cristobalite in opal samples is β phase. It can be seen from

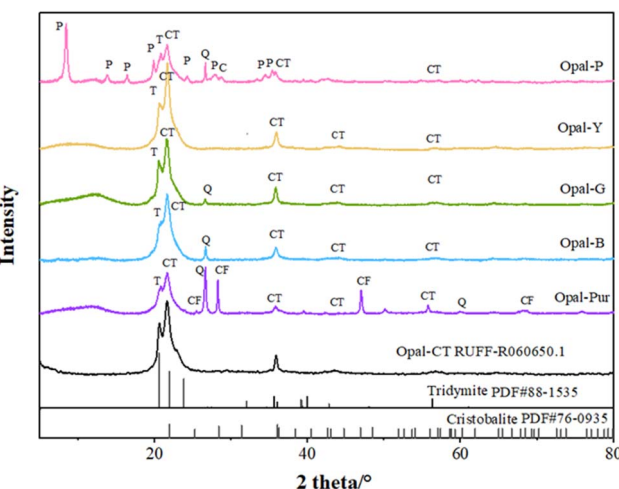


Fig. 4 The XRD patterns of opals with different colors.

Table 2 XRD characteristics of opal samples in this study

Sample	d -Value at 21.6° \AA	C/T ratio (%)	d -Value at 35.8° \AA	FWHM° (2θ)	Structural group	Domain size (nm)
Opal-P	4.110	C0/T100	2.505	0.520	CT	16.5
Opal-Y	4.095	C21/T79	2.498	0.458	CT	18.9
Opal-G	4.106	C6/T94	2.503	0.407	CT	21.4
Opal-B	4.102	C11/T89	2.501	0.471	CT	18.3
Opal-Pur	4.107	C4/T96	2.506	0.526	CT	16.3



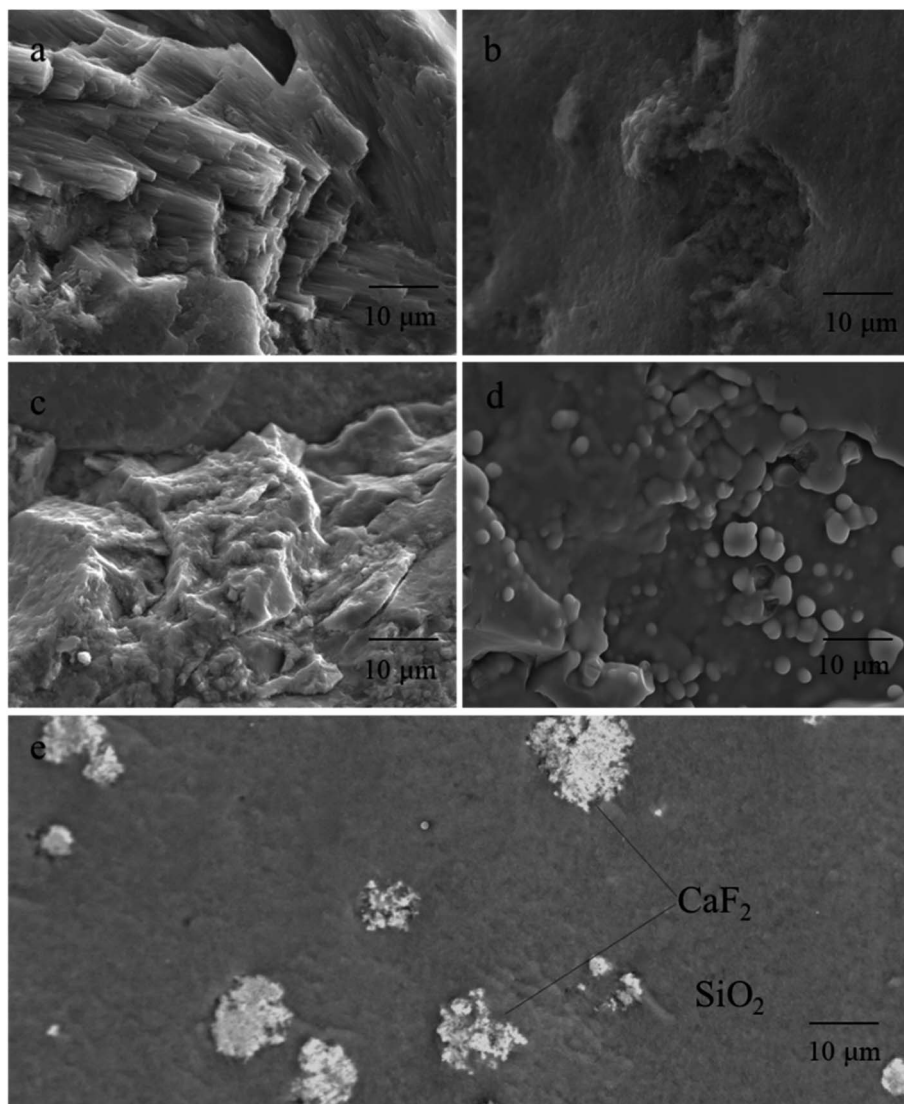


Fig. 5 SEM micrographs of different colored opals. (a) Pink opal; (b) yellow opal; (c) green opal; (d) blue opal; (e) purple opal.

Table 2 that the value of d (4.1 Å) decreases with the increase ratio of cristobalite/tridymite, and the grain size is 16.3–21.4 nm. The FWHM at d (2.5 Å) decreases with the increase of grain size. The higher the crystallinity is, the larger the grain size is. The crystallinity of Opal-G is the highest and that of Opal-Pur is the lowest. With the maturity of crystallinity in mineralogy, it will reflect the gradual sharpening of the main peak and the decrease of FWHH, which further indicates the increase of crystal lattice order.

3.3. SEM/XRF investigation

Generally speaking, CT type opal is a spherical aggregate or fiber crystal composed of lamellar crystals of cristobalite and tridymite, and the matrix is disordered silica.^{46,47} Fig. 5 depicts the SEM micrographs with different scale of the different colored opals.

The microstructure of Opal-P (Fig. 5a) is composed of fibers with a diameter of 0.05–0.1 μm, which are needle-like and

directional columnar in length of 10–30 μm. Combined with XRD and XRF tests (Table 3), the Opal-P is palygorskite rich in Mg and Al, which is consistent with the results verified by Fritsch *et al.*⁴⁸

Opal-Y (Fig. 5b) shows a relatively homogeneous texture. Opal-Y belongs to gel structure, and there are almost no silica spheres. 1–2 microspheres can be seen in some areas, with a size of 0.5 μm, shell-like fracture and small voids.

Opal-G (Fig. 5c) is a massive microstructure composed of silica gel and amorphous silica nanoparticles with unclear boundaries and gaps between blocks. The scale-like structure can be seen in part of the particles in Fig. 5c, and the silica particles exist in the form of blocks with different sizes and shapes.

The microstructure of Opal-B (Fig. 5d) is different from other opals. SiO₂ microspheres with diameters of 1–2 μm can be seen in some areas, and the spheres are all fused with each other. Only when the diameter of the sphere is 0.15–0.3 μm and the gap between the spheres is 0.14–0.24 μm, the grating structure



Table 3 Chemical composition of five different colored opals, obtained by XRF

Sample; mineral	Opal-P	Opal-Y	Opal-G	Opal-B	Opal-Pur
SiO ₂	82.910	94.330	90.620	91.500	83.200
MgO	3.110	0.387	0.070	1.240	1.000
Al ₂ O ₃	2.550	0.147	0.113	0.126	0.325
Fe ₂ O ₃	0.522	0.897	3.520	0.073	0.034
As ₂ O ₃	0.212	0.000	0.000	0.000	0.000
CaO	0.151	0.159	0.205	0.146	6.980
Na ₂ O	0.052	0.076	0.047	0.030	0.000
ZnO	0.045	0.014	0.064	0.138	0.000
MnO	0.040	0.000	0.004	0.000	0.000
CuO	0.038	0.000	0.000	1.960	0.000
SeO ₂	0.037	0.000	0.055	0.045	0.000
Cl	0.031	0.068	0.038	0.065	0.000
TiO ₂	0.023	0.012	0.015	0.006	0.000
P ₂ O ₅	0.021	0.015	0.000	0.000	0.022
Ga ₂ O ₃	0.017	0.016	0.000	0.000	0.000
ZrO ₂	0.013	0.014	0.009	0.012	0.000
Am ₂ O ₃	0.009	0.007	0.009	0.019	0.000
GeO ₂	0.009	0.012	0.000	0.000	0.000
V ₂ O ₅	0.008	0.000	0.003	0.008	0.000
Nb ₂ O ₅	0.006	0.014	0.003	0.008	0.002
Co ₃ O ₄	0.003	0.000	0.002	0.000	0.000
K ₂ O	0.000	0.074	0.038	0.000	0.016
IrO ₂	0.000	0.029	0.000	0.000	0.000
ThO ₂	0.000	0.015	0.011	0.000	0.000
Pr ₆ O ₁₁	0.000	0.013	0.000	0.000	0.000
SrO	0.000	0.004	0.009	0.000	0.016
PbO	0.000	0.000	0.055	0.000	0.000
Nd ₂ O ₃	0.000	0.000	0.008	0.000	0.000
P	0.000	0.000	0.005	0.000	0.000
Cr ₂ O ₃	0.000	0.000	0.004	0.000	0.000
CO ₂	0.000	0.000	0.000	0.000	3.990
F	0.000	0.000	0.000	0.000	4.320
SO ₃	0.000	0.000	0.000	0.000	0.031
U ₃ O ₈	0.000	0.000	0.000	0.000	0.068
Total	89.806	96.302	94.907	95.375	100.004

composed of SiO₂ spheres can diffract visible light, resulting in play of color. Obviously, the size of the silica microsphere in Opal-B is larger than 0.3 μ m, and the external shape of the SiO₂ sphere is irregular. In addition, the boundary between the spheres is not clear, and the gap formed in the three-dimensional space is irregular. Therefore, the play of color effect not occur in Opal-B.

The SEM image of Opal-Pur (Fig. 5e) shows two different colors, indicating that it is composed of two minerals. The matrix material appears gray, showing an uneven surface and the milky structure of spongy unmolded microspheres. The gray-white color has a cluster-shaped microscopic appearance. XRF data (Table 3) show that Opal-Pur contains Ca and F elements. Combined with the magnification observation in Fig. 3 and XRD phase characterization Fig. 4, it is confirmed that the inclusion is purple fluorite.

3.4. Thermogravimetric analysis

Thermogravimetric analysis of all samples was carried out to estimate the water content and dehydration process of opals of

the same type. It can be seen from Fig. 6 that the weight loss rate of the sample from high to low is Opal-P, Opal-G, Opal-Pur, Opal-B and Opal-Y, and the thermal decomposition of all samples can be divided into four stages. The thermal decomposition temperature of each sample and the weight loss rate of each stage are shown in Table 4. The weight loss below 150 °C is molecular water existing on the surface and in open cracks, with a weight loss rate of 0.29–2.36%. Pores water and some hydrogen-bonded water molecules are lost at about 150–350 °C, and the weight loss rate is 0.98–2.9%. Strong hydrogen-bonded water molecules and a small part of silanols are lost at 50–650 °C, and the weight loss rate is 0.36–2.44%. The silanols located in the structure and a small part of the water molecules in the matrix were lost at 1000 °C, and the weight loss rate was 0.22–1.11%. Most of the water in the samples are lost below 650 °C, and the weight loss still exists at 650–1000 °C, at this time, the hydroxyl water located in the structural position is lost. Because of their structural differences, their water content and dehydration temperature are also different.

Opal-P contains a large amount of palygorskite, and palygorskite has large specific surface area, adsorption capacity and strong colloid properties. Therefore, the water content of Opal-P is the highest among the opals, so the weight loss is more than other samples. Opal-Pur contains a lot of CaF₂, and the presence of Ca²⁺ will bond more water molecules.^{49,50} The heating temperature of Opal-Pur is still in a downward trend at 1000 °C, possibly due to the decomposition of calcium fluoride.

3.5. FT-NIR analysis

It is generally believed that most of the water on the surface of opal is not in the form of free water molecules but hydroxyl groups with silicon atoms on the surface of silica to form hydrogen-bonded silanol groups, which is physically adsorbed. The presence of hydrogen-bonded silanol groups is a necessary condition for effective adsorption activity on silica gel surface.⁵¹

It can be seen from Fig. 7 that the absorption peaks of NIR bands of all samples are three regions, which are about 4500 cm⁻¹, 5200 cm⁻¹ and 7000 cm⁻¹. Table 5 summarizes the main attributions of hydration vibration of different colored opal samples in the near infrared region of 8000–4000 cm⁻¹. The peak at 4320 cm⁻¹ is corresponding to bending vibration in siloxane (Si–O–Si) and 4500 cm⁻¹ corresponds to stretching vibration of OH in hydrogen-bonded silanol (Si–OH) and free silanol. The peak at 5060 cm⁻¹ was caused by water molecules bound to silanol groups, while 5230 cm⁻¹ is corresponding to the absorption of free water molecules, which is caused by the bending and stretching vibration of water molecules. The absorption peak around 5200 cm⁻¹ has been proved to distinguish Opal-A and Opal-CT. The wavenumber of Opal-A is generally greater than 5245 cm⁻¹, while Opal-CT was significantly lower than 5240 cm⁻¹.^{12,52} For Opal-CT, the absorption peak intensity at 5200 cm⁻¹ is lower than 5240 cm⁻¹, which is consistent with the study of Langer and Flörke.¹² Bending and stretching vibrations of OH in molecular water and hydrogen-bonded silanol are corresponding to 6830 cm⁻¹ and 7060 cm⁻¹.^{51,53} The wavenumber from 6830 cm⁻¹ and



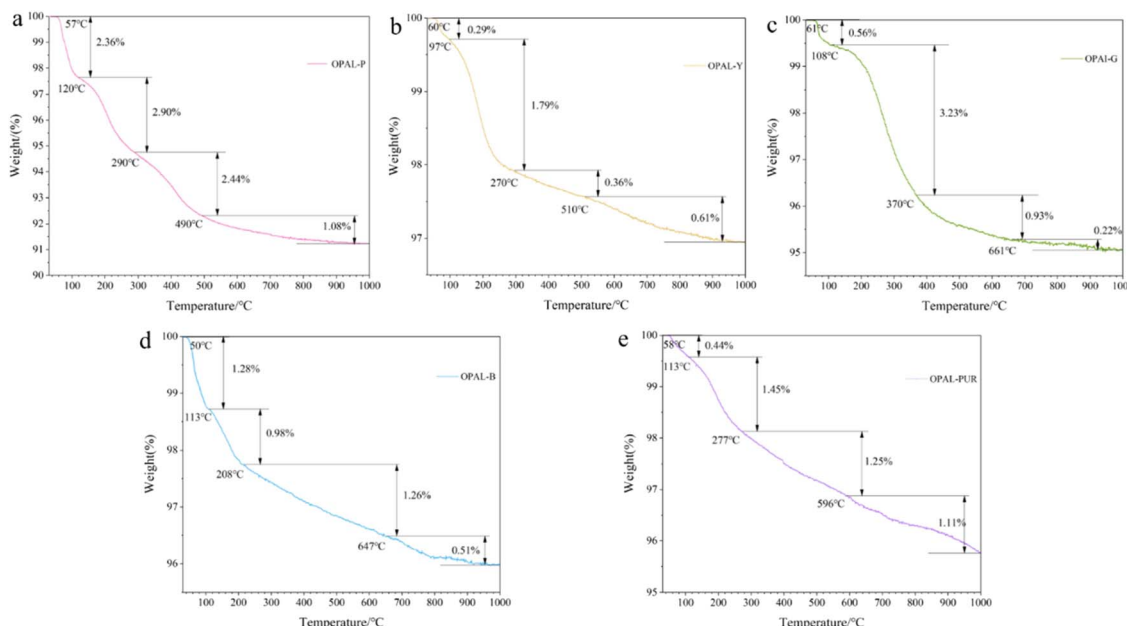


Fig. 6 TG% mass change data plotted as a function of temperature for the opal samples. (a) Pink opal; (b) yellow opal; (c) green opal; (d) blue opal; (e) purple opal.

Table 4 Thermal decomposition temperature and weight loss rate of opal samples with different colors

Sample	$T_1/^\circ\text{C}$	$W_1/\%$	$T_2/^\circ\text{C}$	$W_2/\%$	$T_3/^\circ\text{C}$	$W_3/\%$	Total weight/()
Opal-P	120	2.36	290	2.90	490	2.44	8.78
Opal-Y	97	0.29	270	1.79	510	0.36	3.06
Opal-G	108	0.56	370	3.23	661	0.93	4.94
Opal-B	113	1.28	208	0.98	647	1.26	4.03
Opal-Pur	113	0.43	277	1.45	784	1.81	4.25

7060 cm^{-1} is the combination tone of the vibration in the mid-infrared region. When the peak in this range changes from double peaks to single peak, it indicates a higher degree of hydrogen bonding.^{54–56} The red and blue shift of individual peaks may be due to the difference of microstructure.

The adsorption degree of opal depends on the number of silanol and the proportion of free silanol. The higher the content of silanol groups, the stronger the adsorption capacity. The formation of silanol groups may depend on the depth of occurrence of mineral and the proximity of other free silanol groups on the surface.¹⁶ Generally speaking, the water in opal is composed of molecular water ($\text{H}_2\text{O}_{\text{mol}}$) and silanols ($\text{H}_2\text{O}_{\text{SiOH}}$), and the total water content has been measured by TG. But the distribution and content of water molecules ($\text{H}_2\text{O}_{\text{mol}}$) and silanols ($\text{H}_2\text{O}_{\text{SiOH}}$) in each sample cannot be determined. The absorption bands of molecular water ($\text{H}_2\text{O}_{\text{mol}}$) (5200 cm^{-1}) and silanols ($\text{H}_2\text{O}_{\text{SiOH}}$) (4500 cm^{-1}) in the near infrared region do not overlap. The water content of the two forms can be semi-quantitatively calculated according to these two peaks.^{57,58}

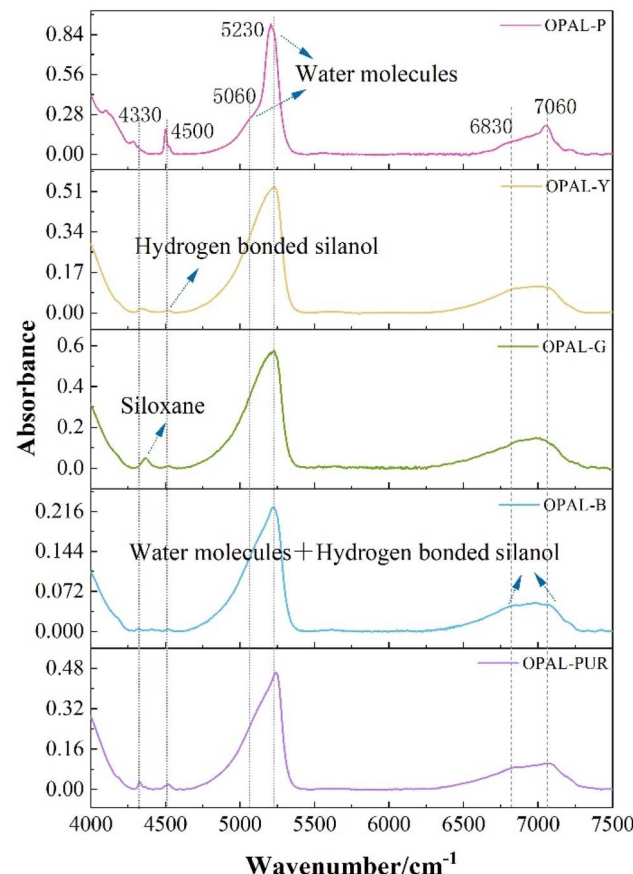


Fig. 7 Near infrared images of opals of different colors.

Table 5 Near infrared characterization of opals of different colors

Peak (cm ⁻¹)	Band assignment
4320	Siloxane (Si—O—Si) bending
4500	Si—OH and siloxane (Si—O—Si) bending
5060	Water molecules hydrogen bonded to silanol groups bending or stretching
5230	Free water molecules bending or stretching
6830	The combination tone of molecular water and silanol groups bending or stretching
7060	

Table 6 Summary of analytical results obtained by TG and FTIR analyses of opal samples

Sample	TG analyses		FTIR analyses	
	H ₂ O _{total} wt%	H ₂ O _{mol} wt%	H ₂ O _{SiOH} wt%	H ₂ O _{total} wt%
Opal-P	8.78	7.03	2.04	9.07
Opal-Y	3.06	3.13	0.07	3.19
Opal-G	4.94	5.02	0.12	5.15
Opal-B	4.03	4.20	0.08	4.18
Opal-Pur	4.25	4.19	0.27	4.41

3400 cm⁻¹ and 3700 cm⁻¹ in the mid-infrared region are caused by the stretching vibration of OH in water and silicone water,^{12,57,59,60} but for minerals with water content greater than 2%, the absorption peaks are unstable and is not suitable for calculation.^{61–63} Therefore, the peak of 5200 cm⁻¹ and 4500 cm⁻¹ is used to semi-quantitatively calculate the water content in opal.

Lambert–Beer law is the basis of quantitative relationship between absorption intensity and absorption substance concentration. The concentrations of H₂O_{SiOH} and H₂O_{mol} were calculated using the Lambert–Beer law (Table 6):

$$w = [18.02 \times \text{Abs}/(d \times \rho \times \varepsilon)] \times 100\%, \quad (1)$$

where w is the H₂O concentration expressed as a weight fraction, Abs is the height of the absorption peak, d is the thickness of the specimen in cm, ρ is the density of the sample in g L⁻¹ and ε is the molar absorptivity (or extinction coefficient) in L mol⁻¹ cm⁻¹. The molar absorptivities is based on the data given by Langer and Flörke (1974).¹² (5200 cm⁻¹: $\varepsilon = 1.14$ L mol⁻¹ cm⁻¹; 4500 cm⁻¹: $\varepsilon = 0.76$ L mol⁻¹ cm⁻¹).

Summary of analytical results obtained by TG and FT-NIR analyses of opal samples is shown in Table 6. Although there are some errors in the total water content and TG test results of NIR test, the changing trend of water content in opal samples is consistent. Potential errors in the FT-NIR analyses may be related to the porosity of the sample, light transmission through the sample, sample thickness and extinction coefficient. The error in this paper is within the range of $\pm 5\%$ for the determination of water content by NIR test. Therefore, the results are still reliable. The content of water molecules (H₂O_{mol}) in all opal

samples are higher than that of silanols (H₂O_{SiOH}), so most of the water in opal is composed of molecular water. These molecular waters (H₂O_{mol}) do not participate in structural construction, exist on the surface, interstitial or in the form of hydrogen-bonded water molecules (H₂O_{mol}). Silanols (H₂O_{SiOH}) are a necessary condition for opal to adsorb, so the higher the amount of silanols (H₂O_{SiOH}), the higher the amount of adsorbed water. The silanols (H₂O_{SiOH}) of Opal-P are the highest, which is caused by the presence of palygorskite. The surface area and adsorption of clay minerals are relatively large, so the water content for Opal-P is the highest, which is consistent with the TG results. Opal-Pur contains a lot of CaF₂, and the presence of Ca²⁺ will bond more water molecules (H₂O_{mol}).^{49,50} Because of the large gap between its structural particles, Opal-G can store water molecules (H₂O_{mol}), which leads to more silanols (H₂O_{SiOH}). The structure of Opal-B is a fused sphere, and these spherical polymers form gaps between which water molecules (H₂O_{mol}) are stored.

4. Conclusions

The structure and water content of five different colored opals were systematically studied in this work. The results showed that all the samples belonged to Opal-CT type. However, there are still some microscopic differences among different color samples. Pink opal is composed of palygorskite fibers with a diameter of 0.05–0.1 μ m. Palygorskite has a large specific surface area, which leads to the most water content for pink opal. Yellow opal contains cloudy inclusions and a relatively homogeneous texture. Green opal has a massive microstructure and a large gap between particles. SiO₂ microspheres with diameters of 1–2 μ m can be seen in some areas of blue opal, and the spheres are all fused with each other. Purple opal is colored by purple fluorite, which shows green fluorescence under long and short wavelength of UV lamp. Purple opal contains more water molecules due to the action of Ca²⁺. The total water content of all samples is ranging from 3.06 to 8.78%. When heated to 1000 °C, the thermal decomposition process of all samples can be divided into four stages, and most of the water in the samples is lost below 650 °C. In addition, this paper introduces the semi-quantitative calculation by using Lambert–Beer law to calculate the content of water molecules (H₂O_{mol}) and silanols (H₂O_{SiOH}) in opals of different colors. The results show that water in five different colored opals mainly exists in the form of molecular water (H₂O_{mol}), and the content of silanols (H₂O_{SiOH}) is less than that of molecular water (H₂O_{mol}). This study brings new data to the understanding of the hydration state of colored opal, especially with respect to content of different forms of water in colored opals.

Author contributions

Niu Li: data collection, writing – original draft; Qingfeng Guo: analysis, review and editing, supervision; Qianqian Wang: software; Libing Liao: data curation; all authors have read and approved the final manuscript.



Conflicts of interest

The authors declare that they have no known competing financial interests or personal relationships that could have appeared to influence the work reported in this paper.

Acknowledgements

Thanks to the School of Gemmology, China University of Geoscience, Beijing.

References

- 1 R. K. Iler, *The occurrence, dissolution, and deposition of Silica*, 1979.
- 2 M. Liesegang, R. Milke, C. Kranz, *et al.*, Silica nanoparticle aggregation in calcite replacement reactions, *Sci. Rep.*, 2017, **7**(1), 14550.
- 3 X. Younan, B. Gates, Y. Yadong, *et al.*, Monodispersed colloidal spheres. Old materials with new applications, *Adv. Mater.*, 2000, **12**(10), 693–713.
- 4 I. Levin and E. Ott, X-Ray Study of Opals, Silica Glass and Silica Gel, *Z. Kristallogr. Cryst. Mater.*, 1933, **85**(1), 305–318.
- 5 J. W. Greig, The Existence of the High-Temperature Form of Cristobalite at Room Temperature and the Crystallinity of Opal, *J. Am. Chem. Soc.*, 1932, **54**(7), 2846–2849.
- 6 R. B. Sosman, The inversion of cristobalite, *J. Am. Chem. Soc.*, 1932, **54**(7), 3015–3016.
- 7 C. V. Raman and A. Jayaraman, The structure of opal and the origin of its iridescence, *Proc. Math. Sci.*, 1953, **38**(2), 101–108.
- 8 O. W. Flörke, Zur Frage des “Hoch-Cristobalit” in Opalen, Bentoniten und Glasern, *Neues Jahrb. Mineral., Monatsh.*, 1955, 217–244.
- 9 C. L. Garavelli, Ordine e disordine opali, *Atti Soc. Toscana Sci. Nat. Pisa, Mem., Ser. A*, 1964, **71**, 133–186.
- 10 J. B. Jones and E. R. Segnit, The nature of opal I. nomenclature and constituent phases, *J. Geol. Soc. Aust.*, 1971, **18**(1), 57–68.
- 11 J. B. Hannay, IV.—Examination of the Hydrous Constituent in Minerals, *Mineral. Mag. J. Mineral. Soc.*, 1877, **(4)**, 106–109.
- 12 K. Langer and O. W. Flörke, Near infrared absorption spectra ($4000\text{--}9000\text{ cm}^{-1}$) of opals and the role of water in these $\text{SiO}_2\cdot\text{nH}_2\text{O}$ minerals, *Fortschr Miner.*, 1974, **52**, 17–51.
- 13 B. Chauvire and P. S. Thomas, DSC of natural opal: insights into the incorporation of crystallisable water in the opal microstructure, *J. Therm. Anal. Calorim.*, 2020, **140**(5), 2077–2085.
- 14 B. Chauvire, C. Boris, B. Rondeau, *et al.*, Near infrared signature of opal and chalcedony as a proxy for their structure and formation conditions, *Eur. J. Mineral.*, 2017, **29**, 409–421.
- 15 P. S. Thomas, *et al.*, Water and hydrogen release from perlites and opal, *J. Therm. Anal. Calorim.*, 2014, **120**, 95–101.
- 16 M. Boboň, A. A. Christy, D. Kluvanec, *et al.*, State of water molecules and silanol groups in opal minerals: a near infrared spectroscopic study of opals from Slovakia, *Phys. Chem. Miner.*, 2011, **38**(10), 809–818.
- 17 A. Smallwood, P. S. Thomas, A. S. Ray, *et al.*, Application of a Fickian model of diffusion to the dehydration of graded specimens of a precious Australian sedimentary opal derived from Coober Pedy, *J. Therm. Anal. Calorim.*, 2009, **(2)**, 685–688.
- 18 R. Day and B. Jones, Variations in water content in opal-A and opal-CT from geyser discharge aprons, *J. Sediment. Res.*, 2008, **(4)**, 301–315.
- 19 J. H. Anderson and K. A. Wickersheim, Near infrared characterization of water and hydroxyl groups on silica surfaces, *Surf. Sci.*, 1964, **2**, 252–260.
- 20 S. G. Bush and J. W. Jorgenson, Confirmation and application of transmission near infrared absorption technique for absolute quantitation of functional groups on silica gel, *J. Chromatogr. A*, 1990, **503**(1), 69–91.
- 21 C. Ghisoli, F. Caucia and L. Marinoni, XRPD patterns of opals: a brief review and new results from recent studies, *Powder Diffr.*, 2010, **25**(3), 274–282.
- 22 E. Fritsch, E. Gaillou, M. Ostroumov, *et al.*, Relationship between nanostructure and optical absorption in fibrous pink opals from Mexico and Peru, *Eur. J. Mineral.*, 2004, **16**(5), 743–751.
- 23 B. M. Laurs and N. D. Renfro, Yellowish Green to Yellow Opal from Brazil, *J. Gemmol.*, 2018, **(3)**, 188–189.
- 24 J. Štubňa and R. Hanus, Yellow Opal from Tanzania, *J. Gemmol.*, 2020, **1**, 10–11.
- 25 F. Caucia, C. Ghisoli, I. Adamo, *et al.*, Opal-C, opal-CT & opal-T from Acari, Peru, *Aust. Gemmol.*, 2008, **6**, 266–271.
- 26 A. Brajkovic, V. Rolandi, P. Vignola, *et al.*, Blue and Pink Opals from Acari, Peru – Their optical, structural and spectroscopic features, *Aust. Gemmol.*, 2007, **23**, 3–15.
- 27 F. Caucia, L. Marinoni, A. Leone, *et al.*, New physical, geochemical and gemological data of opals from Acari Mine (Arequipa Department, Peru), *Neues Jahrb. Mineral., Abh.*, 2015, **192**(1), 73–84.
- 28 M. Hatipoglu, Y. Kibici, G. Yanik, *et al.*, Nano-structure of the cristobalite and tridymite stacking sequences in the common purple opal from the Gevrekseydi deposit, Seyitömer-Kütahya, Turkey, *Orient. J. Chem.*, 2015, **31**(1), 35–49.
- 29 E. Fritsch, B. Mocquet, B. Williams, *et al.*, Purple Fluorite in Opal from Utah, USA, *J. Gemmol.*, 2019, **(5)**, 404–407.
- 30 M. J. Wilson, J. D. Russell and J. M. Tait, A new interpretation of the structure of disordered α -cristobalite, *Contrib. Mineral. Petrol.*, 1974, **47**(1), 1–6.
- 31 D. K. Smith, Evaluation of the detectability and quantification of respirable crystalline silica by X-ray powder diffraction methods, *Powder Diffr.*, 1997, **12**(4), 200–227.
- 32 N. R. Herdianita, P. R. L. Browne, K. A. Rodgers, *et al.*, Mineralogical and textural changes accompanying ageing of silica sinter, *Miner. Deposita*, 2000, **35**(1), 48–62.
- 33 D. E. White, R. A. Hutchinson and T. E. C. Keith, *The Geology and Remarkable Thermal Activity of Norris Geyser Basin*,



Yellowstone National Park, Wyoming, Professional Paper, 1988.

34 O. W. Flörke, H. Graetsch and B. Martin, Nomenclature of Microcrystalline and Noncrystalline Silica Minerals, Based on, *Neues Jahrbuch Fur Mineralogie-Abhandlungen*, 1991, **163**, 19–42.

35 F. A. Caucia, C. A. Ghisoli and I. B. Adamo, A study on the characteristics of some C- and CT-opals from Brazil, *Neues Jahrb. Mineral. Abh.*, 2009, (3), 289–296.

36 F. Caucia, L. Marinoni, V. Bordoni, *et al.*, Physical and chemical properties of some Italian opals, *Period. Mineral.*, 2012, (1), 93–106.

37 F. Caucia, L. Marinoni, A. Leone, *et al.*, Investigation on gemological, physical and compositional properties of some opals from Slovakia (Hungarian opals), *Period. Mineral.*, 2013, **82**(2), 251–261.

38 H. Graetsch, H. Gies and I. Topalović, NMR, XRD and IR study on microcrystalline opals, *Phys. Chem. Miner.*, 1994, **21**(3), 166–175.

39 S. Lee and H. F. Xu, Using powder XRD and pair distribution function to determine anisotropic atomic displacement parameters of orthorhombic tridymite and tetragonal cristobalite, *Acta Crystallogr., Sect. B: Struct. Sci., Cryst. Eng. Mater.*, 2019, **75**(2), 160–167.

40 F. Esenli, I. Kumbasar and V. Esenli, A study on the characteristics of some opals from Turkey, *Neues Jahrb. Mineral. Monatsh.*, 2003, (4), 177–192.

41 F. Esenli, I. Kumbasar, R. H. Eren, *et al.*, Characteristics of opals from Simav, Turkey, *Neues Jahrb. Mineral. Monatsh.*, 2001, 97–113.

42 M. Liesegang and F. Tomaschek, Tracing the continental diagenetic loop of the opal-A to opal-CT transformation with X-ray diffraction, *Sediment. Geol.*, 2020, **398**, 105603.

43 G. D. Guthrie and D. L. Bish, Modeling the X-ray diffraction pattern of opal-CT, *Am. Mineral.*, 1995, (7–8), 869–872.

44 J. García-Rivas, M. Río, E. García-Romero, *et al.*, An insight in the structure of a palygorskite from Palygorskaja: some questions on the standard model, *Appl. Clay Sci.*, 2017, **148**, 39–47.

45 W. C. Ispahring, Discussion of the Occurrence and Origin of Sedimentary Palygorskite-Sepiolite Deposits, *Clays Clay Miner.*, 1973, **21**(5), 391–401.

46 H. A. Graetsch Structural Characteristics of Opaline and Microcrystalline Silica Minerals, *Silica*, 1994.

47 C. Ghisoli, Opals: characterization, nomenclature definition and proposal of a new varieties' classification following the discovery of new materials in Peru, *Scientifica Acta*, 2008, **2**, 27–34.

48 E. Fritsch, M. Ostrooumov and A. Barreau, *et al.*, Mexican Gem Opals: nano-and micro-structure, origin of colour, comparison with other common opals of gemmological significance, *Eleventh Annual V. M. Goldschmidt Conference*, 2002, 3159.

49 J. A. Webb and B. L. Finlayson, Incorporation of Al, Mg, and water in opal-A; evidence from speleothems, *Am. Mineral.*, 1987, **72**, 1204–1210.

50 Z. Karacik, S. C. Genc, F. Esenli, *et al.*, The Gümüldür Fire Opal: Mode of Occurrence and Mineralogical Aspects, *Turk. J. Earth Sci.*, 2011, **1**, 99–114.

51 A. A. Christy, New insight into the surface functionalities and adsorption evolution of water molecules on silica gel surface: a study by second derivative near infrared spectroscopy, *Vib. Spectrosc.*, 2010, **54**(1), 42–49.

52 B. Chauviré, B. Rondeau, F. Mazzero, *et al.*, The Precious Opal Deposit at Wegel Tena, Ethiopia: Formation Via Successive Pedogenesis Events, *Can. Mineral.*, 2017, **55**, 701–723.

53 A. A. Christy, Near infrared spectroscopic characterisation of surface hydroxyl groups on hydrothermally treated silica gel, *Int. J. Chem. Environ. Eng.*, 2011, **2**, 27–32.

54 H. Yamatera, B. Fitzpatrick and G. Gordon, Near infrared spectra of water and aqueous solutions, *J. Mol. Spectrosc.*, 1964, **14**(1), 268–278.

55 G. G. Litvan and R. S. Yamasaki, Simultaneous determination of the spectroscopic and adsorption isotherms of water on silica, *Mater. Constr.*, 1972, (4), 199–207.

56 J. Workman, Practical Guide to Interpretive Near-Infrared Spectroscopy, *Angewandte Chemie*, 2008, **47**, 4628–4629.

57 S. Newman, E. M. Stolper and S. Epstein, Measurement of water in rhyolitic glasses; calibration of an infrared spectroscopic technique, *Am. Mineral.*, 1986, (11–12), 1527–1541.

58 D. M. Dodd and D. B. Fraser, Optical Determinations of OH in Fused Silica, *J. Appl. Phys.*, 1966, **37**(10), 3911.

59 H. Graetsch, O. W. Flörke, *et al.*, The nature of water in chalcedony and opal-C from Brazilian agate geodes, *Phys. Chem. Miner.*, 1985, **12**(5), 300–306.

60 P. L. King, T. W. Vennemann, J. R. Holloway, *et al.*, Analytical techniques for volatiles: A case study using intermediate (andesitic) glasses, *Am. Mineral.*, 2002, (8–9), 1077–1089.

61 G. R. Rossman, Vibrational spectroscopy of hydrous components, *Rev. Mineral. Geochem.*, 1988, (1), 193–206.

62 L. V. Danyushevsky, T. J. Falloon, A. V. Sobolev, *et al.*, The H₂O Content of Basalt Glasses from Southwest Pacific Back-ARC Basins, *Earth Planet. Sci. Lett.*, 1993, (3–4), 347–362.

63 H. Graetsch, Structural characteristics of opaline and microcrystalline silica minerals, *Rev. Mineral. Geochem.*, 1994, (1), 209–232.

